

DISCOVERY OF MASSIVE, MOSTLY STAR-FORMATION QUENCHED GALAXIES WITH EXTREMELY LARGE LYMAN-ALPHA EQUIVALENT WIDTHS AT $Z \sim 3$ *

YOSHIAKI TANIGUCHI¹, MASARU KAJISAWA^{1,2}, MASAKAZU A. R. KOBAYASHI¹, TOHRU NAGAO¹, YASUHIRO SHIOYA¹, NICK Z. SCOVILLE³, DAVID B. SANDERS⁴, PETER L. CAPAK^{3,5}, ANTON M. KOEKEMOER⁶, SUNE TOFT⁷, HENRY J. MCCrackEN⁸, OLIVIER LE FÈVRE⁹, LIDIA TASCA⁹, KARTIK SHETH¹⁰, ALVIO RENZINI¹¹, SIMON LILLY¹², MARCELLA CAROLLO¹², KATARINA KOVAČ¹², OLIVIER ILBERT⁹, EVA SCHINNERER¹³, HAI FU¹⁴, LAURENCE TRESSE⁹, RICHARD E. GRIFFITHS¹⁵, AND FRANCESCA CIVANO¹⁶

Draft version July 3, 2015

ABSTRACT

We report a discovery of 6 massive galaxies with both extremely large Ly α equivalent width and evolved stellar population at $z \sim 3$. These MASSive Extremely Strong Ly α emitting Objects (MAESTLOs) have been discovered in our large-volume systematic survey for strong Ly α emitters (LAEs) with twelve optical intermediate-band data taken with Subaru/Suprime-Cam in the COSMOS field. Based on the SED fitting analysis for these LAEs, it is found that these MAESTLOs have (1) large rest-frame equivalent width of $EW_0(\text{Ly}\alpha) \sim 100\text{--}300 \text{ \AA}$, (2) $M_* \sim 10^{10.5}\text{--}10^{11.1} M_\odot$, and (3) relatively low specific star formation rates of $SFR/M_* \sim 0.03\text{--}1 \text{ Gyr}^{-1}$. Three of the 6 MAESTLOs have extended Ly α emission although they show very compact morphology in the HST/ACS images, which correspond to the rest-frame UV continuum. Since the MAESTLOs do not show any evidence for AGNs, the observed extended Ly α emission is likely to be caused by the superwind activity, suggesting that they are in a final phase of the intense star formation episode. We suggest that this new class of LAEs, MAESTLOs, provides a missing link from star-forming to passively evolving galaxies at the peak era of the cosmic star-formation history.

Keywords: cosmology: observations — early universe — galaxies: formation — galaxies: evolution — galaxies: high-redshift

tani@cosmos.phys.sci.ehime-u.ac.jp

* Based on observations with NASA/ESA *Hubble Space Telescope*, obtained at the Space Telescope Science Institute, which is operated by AURA, Inc., under NASA contract NAS 5-26555; also based on data collected at the Subaru Telescope, which is operated by the National Astronomical Observatory of Japan; and also based on data products from observations made with ESO Telescopes at the La Silla Paranal Observatory under ESO programme ID 179.A-2005 and on data products produced by TERAPIX and the Cambridge Astronomy Survey Unit on behalf of the UltraVISTA consortium.

¹ Research Center for Space and Cosmic Evolution, Ehime University, Bunkyo-cho, Matsuyama 790-8577, Japan

² Graduate School of Science and Engineering, Ehime University, Bunkyo-cho, Matsuyama 790-8577, Japan

³ Department of Astronomy, MS 105-24, California Institute of Technology, Pasadena, CA 91125, USA

⁴ Institute for Astronomy, University of Hawaii, 2680 Woodlawn Drive, Honolulu, HI 96822, USA

⁵ Spitzer Science Center, California Institute of Technology, Pasadena, CA 91125, USA

⁶ Space Telescope Science Institute, 3700 San Martin Drive, Baltimore, MD 21218, USA

⁷ Dark Cosmology Centre, Niels Bohr Institute, University of Copenhagen, Juliane Mariesvej 30, DK-2100 Copenhagen, Denmark

⁸ Institut d'Astrophysique de Paris, UMR7095 CNRS, Université Pierre et Marie Curie, 98 bis Boulevard Arago, 75014, Paris, France

⁹ Aix Marseille Université, CNRS, LAM (Laboratoire d'Astrophysique de Marseille), UMR 7326, 13388, Marseille, France

¹⁰ National Radio Astronomy Observatory, 520 Edgemont Road, Charlottesville, VA 22903, USA

¹¹ Dipartimento di Astronomia, Università di Padova, vicolo dell'Osservatorio 2, 35122, Padua, Italy

¹² Department of Physics, ETH Zurich, 8093, Zurich, Switzerland

¹³ MPI for Astronomy, Königstuhl 17, D-69117 Heidelberg, Germany

¹⁴ Department of Physics & Astronomy, University of Iowa, Iowa City, IA 52245, USA

¹⁵ Physics & Astronomy, STB-216, U. Hawaii at Hilo, Hilo, HI 96720, USA

¹⁶ Yale Center for Astronomy and Astrophysics, 260 Whitney Avenue,

New Haven, CT 06520, USA; Smithsonian Astrophysical Observatory, 60 Garden Street, Cambridge, MA 02138, USA

1. INTRODUCTION

Most of massive galaxies in the present universe are passively evolving galaxies with little on-going star formation (e.g., Kauffmann et al. 2003). In the current understanding of galaxy evolution, massive galaxies are considered to have evolved more rapidly than less massive systems in earlier universe: so-called the downsizing evolution of galaxies (Cowie et al. 1996). These massive galaxies have formed their stars actively by a cosmic age of a few Gyr (redshift $z \sim 2-3$), when the cosmic star formation rate density peaked (e.g., Bouwens et al. 2011). After this epoch, their star formation stopped and they passively evolved into elliptical galaxies seen today. However, the quenching mechanism of star formation in these massive galaxies has not yet been understood because the process may have occurred in a relatively short time scale, making it difficult to observe such events (e.g., Renzini 2009; Peng et al. 2010; Durkalec et al. 2015; Mancini et al. 2015).

To seek for star-forming galaxies in young universe, the Hydrogen Ly α emission provides the most useful tool. Therefore, many searches for redshifted Ly α emission have resulted in the discovery of young galaxies beyond $z \sim 7$, corresponding to an cosmic age of $\lesssim 750$ Myr (Ono et al. 2012; Shibuya et al. 2012; Finkelstein et al. 2013; Konno et al. 2014; Schenker et al. 2014). Among such Ly α emitting galaxies (Ly α emitters, hereafter LAEs), those with a very large equivalent width (EW), i.e., extremely strong LAEs, are particularly important in that they can be galaxies in a very early stage of galaxy formation (e.g., Schaerer 2003; Nagao et al. 2007).

In order to search for them, we have carried out a survey for extremely strong LAEs over an unprecedentedly large volume. While most of the detected objects with strong Ly α seem to be young galaxies with small stellar mass as expected for LAEs, we have serendipitously found 6 massive galaxies with extremely large EW(Ly α) and relatively evolved stellar population at $z \sim 3$, that show no evidence for an active galactic nucleus (AGN). Here we present the physical properties of this new population that is expected to be in a transition phase between star-forming and passive evolution. In this Letter, we use a standard cosmology with $\Omega_M = 0.3$, $\Omega_\Lambda = 0.7$, and $H_0 = 70 \text{ km s}^{-1} \text{ Mpc}^{-1}$.

2. DATA AND ANALYSIS

In this study, we use the multi-wavelength data set from the Cosmic Evolution Survey (COSMOS; Scoville et al. 2007). Optical imaging data with 12 intermediate-band (hereafter, IA-band) filters equipped on Subaru/Suprime-Cam allow us to pick up strong emission-line objects by a significant flux excess in one of the IA bands. The spectral resolution of our IA filters is $R = \lambda/\Delta\lambda = 20-26$, and the 12 IA filters cover the whole optical wavelength range from 4270 Å to 8270 Å (Taniguchi et al. 2015). Therefore, we can search for strong LAEs at $2.5 < z < 5.8$. Although the details of our selection procedure for strong LAEs are given elsewhere (M. A. R. Kobayashi et al., in prep.), we briefly summarize it in the following.

At first, from the COSMOS Official Photometric Catalog (version 2012, Capak et al. 2007), we selected objects with a significant (3σ) flux excess in an IA band from the frequency-matched continuum estimated by using two adjacent broad-band magnitudes. In order to identify which emission line causes the IA-band excess of these objects, we applied the public photometric redshift code EAZY (Brammer

et al. 2008) to the multi-band photometric data from optical to MIR, which include CFHT u^* and i^* , Subaru $Bg'Vr'i'z'$ and 12 IA bands (Taniguchi et al. 2007), UltraVISTA $YJHK$ (McCracken et al. 2012), and Spitzer/IRAC 3.6 μm and 4.5 μm bands (Sanders et al. 2007). The excess IA band and any broad bands whose wavelength coverage is overlapped with the excess IA band are excluded from the photometric redshift calculation. We adopted a line identification with the highest probability in the volume-weighted redshift likelihood function, and assigned the photometric redshift assuming the emission line enters into the effective wavelength of the excess IA band. We selected LAEs from these strong emission-line objects and then performed the spectral energy distribution (SED) fitting with the GALAXEV population synthesis model (Bruzual & Charlot 2003) to estimate the physical properties of the LAEs. In the SED fitting, we assumed the exponentially decaying star formation histories with an e -folding timescale of $\tau = 0.01-10$ Gyr. The Chabrier initial mass function (Chabrier 2003) and the Calzetti extinction law (Calzetti et al. 2000) were adopted. The excess IA band and any broad bands overlapping with the excess band were again excluded. Although other strong emission lines such as [O II], [O III], and H α may enter into the JHK bands, we used all JHK -band data in the fitting, because the effect of such emission lines is not expected to be serious for these bands with wide filter bandpasses. In addition to the multi-band photometry used in the photometric redshift estimate, we also used the IRAC 5.8 μm and 8.0 μm bands to obtain more accurate physical properties such as the stellar mass and age. Our survey covers a 1.34 deg² area in the COSMOS field, that is, the overlapped area between COSMOS deep region and UltraVISTA DR1 (McCracken et al. 2012). The wide survey area and wide wavelength coverage of the 12 IA bands allow us to search for strong LAEs at $2.5 < z < 5.8$ over a very large volume of $5.5 \times 10^7 \text{ Mpc}^3$.

As a result, we obtain a sample of 589 LAEs at $2.5 < z < 5.3$. In this sample, 18 LAEs have both an extremely large rest-frame equivalent width of $EW_0(\text{Ly}\alpha) \geq 100 \text{ \AA}$ and a large stellar mass with $M_* \geq 10^{10.5} M_\odot$. Hereafter, we call these 18 LAEs MAssive, Extremely STRong Ly α emitting Objects (MAESTLOs). Since our main interest is the star-forming activity in galaxies, we rejected possible active galactic nuclei (AGN) by using the IRAC color criteria proposed by Donley et al. (2012). We also used the XMM-COSMOS (Hasinger et al. 2007), Chandra-COSMOS (Elvis et al. 2009; Civano et al. 2012) and Chandra COSMOS Legacy (F. Civano et al., in prep.) and VLA-COSMOS (Schinnerer et al. 2007) catalogues to reject AGNs. In total, 12 MAESTLOs turn out to show evidence for AGN. Accordingly, we obtain a sample of 6 MAESTLOs without evidence for AGN¹⁸. Their observational properties are summarized in Table 1.

Their sizes are measured in the excess IA-band (i.e., Ly α image) and the COSMOS HST/ACS I_{F814W} -band mosaics (Koekemoer et al. 2007), corresponding to the rest-frame UV continuum, by using the GALFIT code (Peng et al. 2002). We fit the observed surface brightness with an exponential law, taking account of the point spread function (PSF) of these data. We chose to fix the Sérsic index to $n = 1$ because our

¹⁸ Note that a stacking analysis for the 6 MAESTLOs, corresponding to a ~ 650 ksec exposure, results in no detection. The 95% upper limit in the 0.5–2 keV band is $3.63 \times 10^{-5} \text{ counts s}^{-1}$ which corresponds to a rest-frame luminosity of $7.76 \times 10^{42} \text{ ergs s}^{-1}$ at $z \sim 3$.

Table 1
Physical Properties of the 6 MAESTLOs

No.	z_{phot}	$\log M_*$ (M_{\odot})	τ (Gyr)	age (Gyr)	$E(B-V)$ (mag)	$EW_0(\text{Ly}\alpha)$ (\AA)	$\log[SFR/(M_{\odot} \text{ yr}^{-1})]$	
							Ly α	SED
1	3.16	$11.11^{+0.08}_{-0.00}$	$0.32^{+0.08}_{-0.00}$	$1.61^{+0.29}_{-0.18}$	$0.03^{+0.06}_{-0.00}$	240^{+20}_{-19}	$1.12^{+0.02}_{-0.02}$	$0.63^{+0.26}_{-0.00}$
2	2.81	$11.11^{+0.04}_{-0.07}$	$1.59^{+1.58}_{-0.59}$	$1.80^{+0.40}_{-0.52}$	$0.29^{+0.03}_{-0.02}$	306 ± 20	$1.20^{+0.02}_{-0.02}$	$1.79^{+0.12}_{-0.08}$
3	2.81 ^a	$10.90^{+0.00}_{-0.00}$	$0.05^{+0.00}_{-0.00}$	$0.29^{+0.00}_{-0.00}$	$0.19^{+0.00}_{-0.00}$	171 ± 6	$1.04^{+0.02}_{-0.02}$	$0.89^{+0.00}_{-0.00}$
4	3.24	$10.71^{+0.12}_{-0.03}$	$0.40^{+0.40}_{-0.00}$	$1.28^{+0.62}_{-0.14}$	$0.12^{+0.05}_{-0.04}$	178 ± 16	$0.88^{+0.03}_{-0.03}$	$0.94^{+0.22}_{-0.16}$
5	2.50 ^b	$10.54^{+0.08}_{-0.04}$	$0.06^{+9.94}_{-0.02}$	$0.14^{+0.26}_{-0.03}$	$0.40^{+0.04}_{-0.03}$	107^{+11}_{-14}	$0.68^{+0.03}_{-0.03}$	$1.94^{+0.37}_{-0.27}$
6	3.16	$10.52^{+0.03}_{-0.03}$	$0.50^{+0.00}_{-0.00}$	$1.90^{+0.00}_{-0.10}$	$0.02^{+0.02}_{-0.01}$	124 ± 16	$0.64^{+0.05}_{-0.05}$	$0.41^{+0.08}_{-0.03}$

Note. — The No. is given in order of decreasing the estimated stellar mass. Errors for the quantities correspond to 1- σ confidence interval (i.e., $\Delta\chi^2 \leq 1$) estimated from the SED fitting. In the SED fitting, the templates older than cosmic age at z_{phot} are not used. The entry of 0.00 for these errors indicate that there is no parameter grid in $\Delta\chi^2 \leq 1$ around the best-fit model parameter.

^a $z_{\text{spec}} = 2.798$.

^b $z_{\text{spec}} = 2.513$.

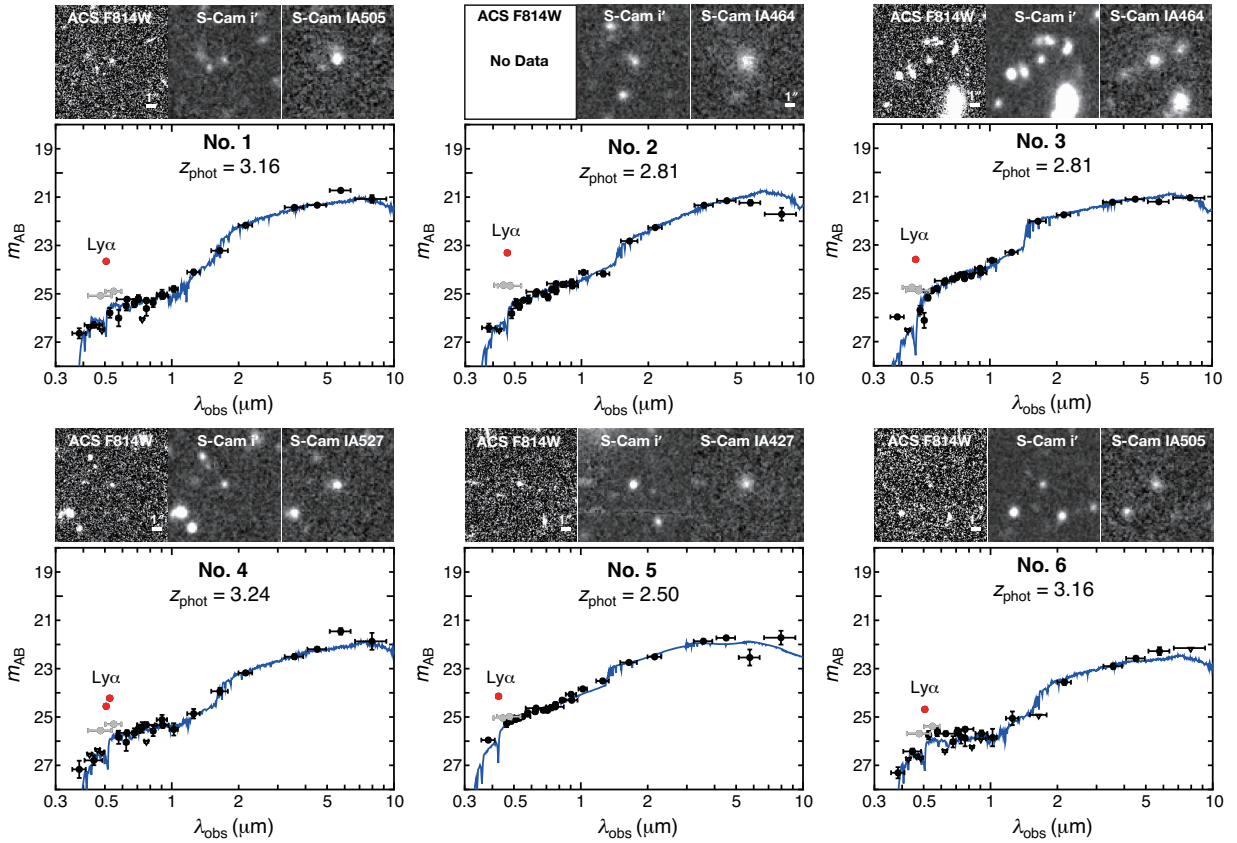


Figure 1. SEDs and HST and Subaru images of the 6 MAESTLOs. In the bottom main panel, the observed data points are shown by filled circles with error bars. The red symbol shows the IA band with a significant flux excess by the Ly α emission, while the grey symbols represent the broad bands whose wavelength coverage overlaps with the excess IA band. The blue curve shows the best-fit model SED from the GALAXEV library. The data affected by the strong Ly α emission (red and grey points) are not used in the SED fitting. The inverted triangles represents the 3σ upper limit for the undetected bands. In the top panels, the thumbnails of the HST ACS in the F814W filter, the Subaru Suprime-Cam i' -band image, and the excess IA-band image are shown. Each panel is $12'' \times 12''$ in size. The ACS images are convolved with a Gaussian kernel with $\sigma = 1$ pix ($= 0''.03$) to reduce the noise.

Table 2
Size measurements of the 6 MAESTLOs

No.	ACS F814W		S-Cam i'		S-Cam IA	
	r_{HL} (kpc)	f_{unres}	r_{HL} (kpc)	f_{unres}	r_{HL} (kpc)	f_{unres}
1	0.52 ± 0.08	0.060	$< 3.87^{\text{b}}$	0.660	4.50 ± 0.61	0
2	— ^a	— ^a	4.49 ± 2.01	0.175	6.68 ± 0.70	0
3	1.00 ± 0.09	0	4.21 ± 1.75	0.115	7.18 ± 0.80	0
4	0.34 ± 0.12	0.100	$< 3.83^{\text{b}}$	0.750	$< 6.20^{\text{b}}$	0.685
5	$< 0.57^{\text{b}}$	0.880	$< 4.12^{\text{b}}$	0.710	3.77 ± 1.83	0.050
6	$< 0.54^{\text{b}}$	0.645	$< 3.87^{\text{b}}$	0.670	$< 5.74^{\text{b}}$	0.410

Note. — r_{HL} is half-light radius and f_{unres} is Errors for r_{HL} are based on the Monte Carlo simulation described in the text.

^a Out of the ACS/F814W-band data.

^b Unresolved.

data are not deep enough to resolve the degeneracy between the radius and Sérsic index for MAESTLOs. The PSF images of the excess IA-band and ACS data are measured by combining relatively bright isolated stars in each image. Note, however, that we cannot measure the ACS sizes for MAESTLO No. 2 since this object is out of the HST/ACS field. Furthermore, we also measure the sizes of the rest-frame UV continuum using the i' -band data taken with the same instrument as that of the excess IA-band data. Note that the half light radius of the PSF in the excess IA bands is 0.75–0.83 arcsec, while that in the i' band is 0.51 arcsec. In order to estimate the uncertainty in the size measurements including the systematic effects such as the background fluctuation, we carry out the Monte Carlo simulation as in previous studies (e.g., Straatman et al. 2015). After adding the best-fit model profile to the image at 200 random positions around the original position (in a $2' \times 2'$ region), we re-measure their sizes. The standard deviation of these 200 measurements is adopted as the size uncertainty. In order to check whether the object is significantly extended or not, we also calculated the fraction of the cases that GALFIT returned the “unresolved” flag, f_{unres} , in the 200 measurements. The estimated half-light radii and errors of the MAESTLOs together with f_{unres} are given in Table 2.

3. RESULTS & DISCUSSIONS

In Figure 1, we show the rest-frame UV–NIR SED of the 6 MAESTLOs together with their thumbnails in the excess IA, i' , and ACS I_{F814W} bands. It is found that they are significantly bright in the rest-frame NIR wavelengths, leading to their large estimated stellar masses of $\log(M_*/M_\odot) = 10.5$ – 11.1 . Another unexpected property is that they show very red rest-frame UV-optical colors despite of their extremely large $EW_0(\text{Ly}\alpha)$; i.e., the MAESTLOs show a relatively strong 4000 Å continuum break in the rest-frame optical as well as the Lyman break in the rest-frame far-UV. These continuum features allow us to identify the flux excess in a concerned IA band as the $\text{Ly}\alpha$ emission line, resulting in an accurate photometric redshift for them. In fact, two of the 6 MAESTLOs have spectroscopic identifications and their spectroscopic redshifts agree with the photometric redshifts estimated from the IA-band excess (Nos. 3 and 5; see Table 1). The strong 4000 Å break observed in the MAESTLOs suggests relatively old stellar population in them, and their best-fit stellar ages based on SED fitting are 1–2 Gyr¹⁹. Thus these galaxies form

¹⁹ Note that 2 MAESTLOs (i.e., Nos. 3 and 5) have relatively young ages. No. 3 has a very short e -folding timescale and a clear Balmer break in the

a completely different population from typical high-redshift LAEs with small stellar masses and young stellar ages (e.g., Ono et al. 2010; Hagen et al. 2014).

Despite their relatively old stellar population, the MAESTLOs have extremely large $EW_0(\text{Ly}\alpha)$ of ~ 100 – 300 Å. In order to compare the star formation rates (SFR) estimated from $\text{Ly}\alpha$ luminosity, $SFR(\text{Ly}\alpha)$, with that from SED fitting, $SFR(\text{SED})$, we show $SFR(\text{Ly}\alpha)/SFR(\text{SED})$ ratios of the MAESTLOs as a function of stellar mass in the top panel of Figure 2. Here, we use the Kennicutt (1998) relation between SFR and $L(\text{H}\alpha)$ combined with both the $L(\text{Ly}\alpha)/L(\text{H}\alpha)$ ratio of 8.7 under the case B recombination and a correction factor converting from the Salpeter IMF into the Chabrier IMF (i.e., multiplied by a factor of 0.60). For typical LAEs, it is found that the SFR ratio decreases with increasing stellar mass (Hagen et al. 2014). On the other hand, for most MAESTLOs, $SFR(\text{Ly}\alpha)$ is comparable to $SFR(\text{SED})$ and thus their SFR ratios are similar to those of typical LAEs with much smaller masses. Therefore, it is suggested that the escape fraction of the $\text{Ly}\alpha$ emission is relatively high in these galaxies and/or that there are other additional energy sources besides the photoionization by massive OB stars.

We infer that the observed extremely large $EW_0(\text{Ly}\alpha)$ is attributed to a large-scale superwind surrounding the MAESTLOs. The shock heating associated with the outflowing gas can produce the additional $\text{Ly}\alpha$ emission because such supernova-driven shocks can provide a significantly high $\text{Ly}\alpha$ luminosity, which is comparable to the photoionization by young massive stars (e.g., Mori & Umemura 2006). Furthermore, if the high-velocity gas outflows are induced by supernova feedback, a large fraction of $\text{Ly}\alpha$ photons in these MAESTLOs can escape from the galaxy itself (e.g., Kunth et al. 1998). Indeed, three of the 6 MAESTLOs (Nos. 1, 2, and 3) have extended $\text{Ly}\alpha$ emission in the excess IA band, while all the MAESTLOs are compact in the both ACS I_{F814W} -band and Subaru i' -band data. The half-light radius of these three MAESTLOs in the IA-band data is ~ 4 – 7 kpc, while that in the ACS data is ≤ 1 kpc for all the MAESTLOs (Table 2). We also note that all the MAESTLOs cannot be distinguished from the point sources in the Subaru i' -band data (see f_{unres} in Table 2), which is consistent with the very small sizes in the ACS data. In order to investigate the effect of the relatively worse spatial resolution of the IA-band data, we carried out the similar simulations in the IA-band data as mentioned in Section 2. We convolved the model galaxies with the size and axial ratio measured in the ACS (rest-frame UV continuum) data with the PSF of the IA-band data and added them into the IA-band image. Then the sizes of these model galaxies were measured by GALFIT. We performed 200 such simulations for MAESTLO Nos. 1 and 3, which show the extended $\text{Ly}\alpha$ emission²⁰, and found that GALFIT returned the “unresolved” flag in most cases (185/200 and 169/200 for MAESTLO Nos. 1 and 3, respectively). On the other hand, f_{unres} is 0/200 for the observed $\text{Ly}\alpha$ emission (the IA band) of these MAESTLOs (Table 2). Therefore we conclude that the $\text{Ly}\alpha$ emission of these MAESTLOs is significantly extended relative to the rest-frame UV continuum.

As for possible origins of the observed extended $\text{Ly}\alpha$ emis-

SED, suggesting that its SFR is rapidly decreasing. On the other hand, No. 5 shows relatively weak Balmer/4000 Å break compared to the other MAESTLOs and its e -folding timescale is highly uncertain.

²⁰ MAESTLO No. 2 also shows the extended $\text{Ly}\alpha$ emission, but the ACS data are not available for this object (Section 2).

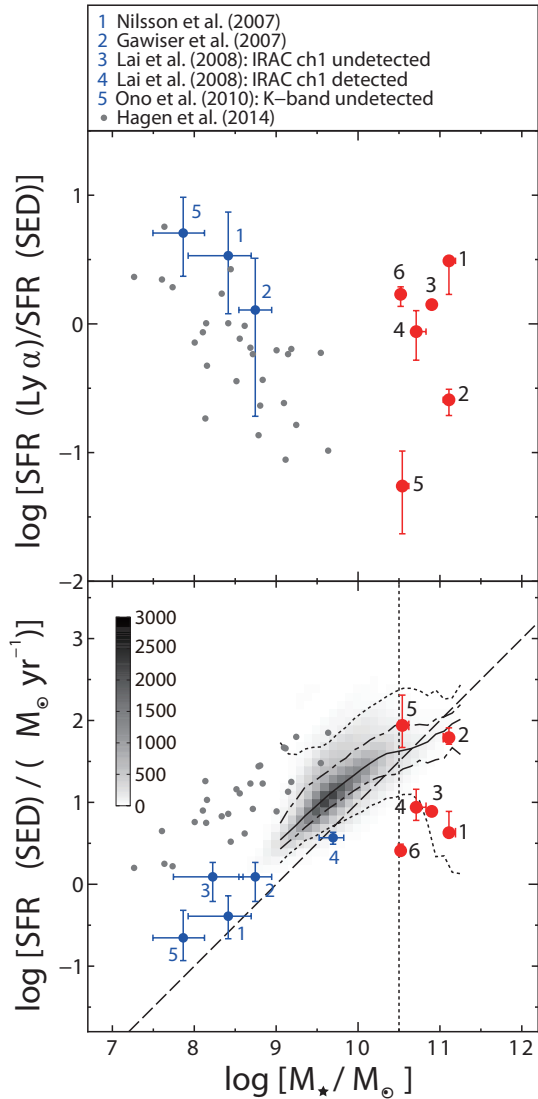


Figure 2. $SFR(Ly\alpha)/SFR(SED)$ vs. M_* (top) and $SFR(SED)$ vs. M_* (bottom) for our MAESTLOs (red circles) and LAEs at $z \sim 3$ from the literatures (blue and gray circles for the results from stacked LAEs and from individual LAE, respectively). For Hagen et al. (2014), we plot only the LAEs at $z = 2.5\text{--}3.2$ in their sample. Note that the SFRs and M_* in the literatures derived with the Salpeter IMF are converted into those with the Chabrier IMF we use. Note also that Hagen et al. (2014) used the SFRs estimated from the dust-corrected UV luminosity instead of those based on the SED fitting. In the bottom panel, we also plot the so-called main sequence of star-forming galaxies at $z_{\text{phot}} = 2.5\text{--}3.2$ in the COSMOS field in gray scale with bin size of 0.1 dex in M_* and SFR. The scale (the number of galaxies per bin) is shown in the upper-left inset. Solid, dot-dashed, and dotted lines show the median, 16 and 84 percentiles, and 2.5 and 97.5 percentiles in bins of 0.1 dex in stellar mass. The dashed line shows the relation of $sSFR = 1 \text{ Gyr}^{-1}$. The vertical dotted line corresponds to $\log(M_*/M_\odot) = 10.5$, which is one of the criteria of MAESTLO.

sion, we may have a projection effect. However, we consider that such a projection effect cannot be the origin of most MAESTLOs because of the small number densities of both massive galaxies with relatively low $sSFR$ and LAEs with extremely large EWs at $z \sim 3$ (e.g., $\sim 1.3 \times 10^{-5} \text{ Mpc}^{-3}$ for galaxies with $M_* \geq 10^{10.5} M_\odot$ and $sSFR = 0.03\text{--}0.3 \text{ Gyr}^{-1}$, and $\sim 5.4 \times 10^{-6} \text{ Mpc}^{-3}$ for LAEs with $EW_0(Ly\alpha) \geq 100 \text{ \AA}$). Namely, the projection probability of these objects with similar redshifts (e.g., $\Delta z < 0.5$) is expected to be extremely low (~ 0.003 such chance alignments within $1''$ in our survey vol-

ume). Another possibility is that a star-forming dwarf galaxy is going to merge onto these MAESTLOs. In this case, we have to explain why a merging dwarf galaxy experiences such active star formation. Finally, jets and/or outflows from AGN are also possible origins of such extended emission-line regions. However, our MAESTLO sample does not show any evidence for AGNs (Section 2), although weak AGN possibility is not completely rejected because of the limited depths of IRAC, XMM, Chandra, and radio data.

In order to investigate their evolutionary stage, we show the distribution of MAESTLOs in the $SFR(SED)\text{--}M_*$ plane together with typical LAEs at $z \sim 3$ (Nilsson et al. 2007; Gawiser et al. 2007; Lai et al. 2008; Ono et al. 2010; Hagen et al. 2014) and galaxies at $z_{\text{phot}} = 2.5\text{--}3.2$ in the COSMOS field (bottom panel of Figure 2). Compared to normal star-forming galaxies on the main sequence at similar stellar masses and redshifts, the MAESTLOs have a smaller specific SFR^{21} , $sSFR = SFR/M_* \sim 0.03\text{--}1 \text{ Gyr}^{-1}$, suggesting that their star formation activities are just ceasing and that they are in a transition phase from actively star-forming into quiescent galaxies. This contrasts with normal LAEs that tend to have a $sSFR$ similar with or higher than main-sequence galaxies (e.g., Hagen et al. 2014).

In order to complementarily investigate the star formation histories of the MAESTLOs, we show the rest-frame $U\text{--}V$ vs. $V\text{--}J$ diagram in Figure 3. Comparing the quiescent galaxies studied by Muzzin et al. (2013), we find that our four MAESTLOs with a low $sSFR$ (Nos. 1, 3, 4, and 6) are located around the selection boundary for the quiescent galaxies and that their colors are consistent with the model tracks where star formation has been recently quenched. Therefore, this color analysis reinforces our scenario, suggesting that they have been recently quenched and are moving into the passive evolution phase. Although the colors of the other two MAESTLOs are consistent with the star-forming models, their colors can also be interpreted as a galaxy that ceased its star formation recently. The larger dust contents in these two galaxies may be expected if they are in an early phase of the superwind activity; i.e., most of dust grains may have not yet been blown out by the superwind. We thus infer that MAESTLOs are in the final stage of massive galaxy formation where their SFRs decrease as gas is ejected from the galaxy as the superwind.

If the sizes in the rest-frame UV continuum represent the stellar mass distribution of MAESTLOs, their sizes are very similar to those of compact massive quiescent galaxies found at $z \sim 2$ (van der Wel et al. 2014), implying that the MAESTLOs can be interpreted as their progenitors. It has been recently suggested that massive compact star-forming galaxies at $z \sim 2\text{--}3$ evolve into compact quiescent galaxies after the cease of their star formation (e.g., Barro et al. 2013). Although they are mostly dusty galaxies whose sizes are as small as the MAESTLOs, they have a younger age of $1.1^{+0.2}_{-0.6} \text{ Gyr}$ and a higher $sSFR$ of $0.3\text{--}3 \text{ Gyr}^{-1}$ than MAESTLOs (Barro et al. 2014). We therefore suggest that they will evolve to passive galaxies through the MAESTLO phase.

Our survey volume ($z = 2.42\text{--}2.59$ and $2.72\text{--}3.42$) corresponds to $1.4 \times 10^7 \text{ Mpc}^3$ and the number density of MAESTLOs is $4.3 \times 10^{-7} \text{ Mpc}^{-3}$ ($2.9 \times 10^{-7} \text{ Mpc}^{-3}$ if we ex-

²¹ One exception is MAESTLO No. 5, which has a weak Balmer break as mentioned above. Its $sSFR$ is consistent with the main sequence at the redshift.

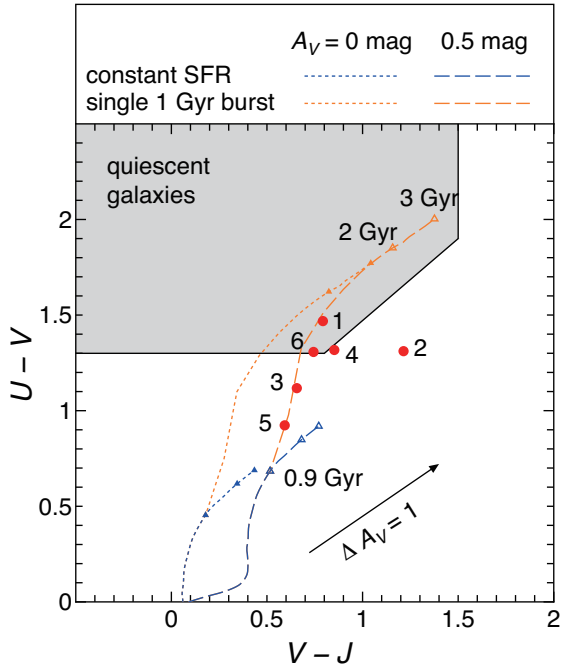


Figure 3. Rest-frame $U - V$ vs. $V - J$ two-color diagram for the MAESTLOs. The 6 MAESTLOs are shown by filled circles with their ID numbers. The domain of quiescent galaxies studied by Muzzin et al. (2013) is shown with the gray shaded area. Two star formation models (the constant star formation and the single 1 Gyr starburst) are also shown by blue and orange dotted curves for $A_V = 0$ and by blue and orange dashed curves for $A_V = 0.5$ mag.

clude MAESTLOs Nos. 2 and 5 with a relatively high sSFR). Thus MAESTLOs may have been missed by previous narrow-band surveys because their survey volumes were insufficient even in a survey with powerful instruments such as Subaru/Suprime-Cam (e.g., Ouchi et al. 2008).

Here we compare the number density of MAESTLOs with star-forming and quiescent galaxies with $M_* > 10^{10.5} M_\odot$ using the stellar mass function of galaxies at the same redshift range (Ilbert et al. 2013). We then find that the MAESTLOs constitute only 0.2–0.6% of star-forming galaxies and $\sim 2\%$ of quiescent galaxies. If we assume that all galaxies with $M_* > 10^{10.5} M_\odot$ pass the phase of MAESTLO when they evolve from star-forming to quiescent galaxies, we obtain the duration of this phase, $\sim 0.02 \times t_{\text{univ}} (z \sim 3-4) \sim 30-50$ Myr ($\sim 20-34$ Myr if we exclude Nos. 2 and 5), making them a rare population. Such a short timescale truncation has been recently discussed based on other observational properties of galaxies at $z \sim 3$ (Durkalec et al. 2015; Mancini et al. 2015).

How the star formation was quenched in high-redshift massive galaxies is now the most important issue for understanding galaxy formation and evolution. Detailed observations of MAESTLOs such as integral field spectroscopy and large volume surveys for such massive galaxies with extremely large $EW_0(\text{Ly}\alpha)$ by, for example, ALMA and Subaru/Hyper Suprime-Cam will allow us to study their gas kinematics and

reveal the physical mechanisms of quenching (e.g., strong stellar/supernova feedback with outflows or strangulation/gas consumption) in massive galaxies in the early universe.

We would like to thank both the Subaru and HST staff for their invaluable help, and all members of the COSMOS team. We would also like to thank the anonymous referee for valuable suggestions and comments. We also thank Alex Hagen for kindly providing us with the information of their LAEs. This work was financially supported in part by JSPS (YT: 15340059, 17253001, 19340046, and 23244031; TN: 23654068 and 25707010).

REFERENCES

- Barro, G., Faber, S. M., Pérez-González, P. G., et al. 2013, *ApJ*, 765, 104
 Barro, G., Faber, S. M., Pérez-González, P. G., et al. 2014, *ApJ*, 791, 52
 Bouwens, R. J., Illingworth, G. D., Labbe, I., et al. 2011, *Nature*, 469, 504
 Brammer, G. B., van Dokkum, P. G., & Coppi, P. 2008, *ApJ*, 686, 1503
 Bruzual, G., & Charlot, S. 2003, *MNRAS*, 344, 1000
 Calzetti, D., Armus, L., Bohlin, R. C., et al. 2000, *ApJ*, 533, 682
 Capak, P., Aussel, H., Ajiki, M., et al. 2007, *ApJS*, 172, 99
 Chabrier, G. 2003, *PASP*, 115, 763
 Civano, F., Elvis, M., Brusa, M., et al. 2012, *ApJS*, 201, 30
 Cowie, L. L., Songaila, A., Hu, E. M., & Cohen, J. G. 1996, *AJ*, 112, 839
 Donley, J. L., Koekemoer, A. M., Brusa, M., et al. 2012, *ApJ*, 748, 142
 Durkalec, A., Le Fèvre, O., de la Torre, S., et al. 2015, *A&A*, 576, L7
 Elvis, M., Civano, F., Vignali, C., et al. 2009, *ApJS*, 184, 158
 Finkelstein, S. L., Papovich, C., Dickinson, M., et al. 2013, *Nature*, 502, 524
 Gawiser, E., Francke, H., Lai, K., et al. 2007, *ApJ*, 671, 278
 Hagen, A., Ciardullo, R., Gronwall, C., et al. 2014, *ApJ*, 786, 59
 Hasinger, G., Cappelluti, N., Brunner, H., et al. 2007, *ApJS*, 172, 29
 Ilbert, O., McCracken, H. J., Le Fèvre, O., et al. 2013, *A&A*, 556, A55
 Kauffmann, G., Heckman, T. M., White, S. D. M., et al. 2003, *MNRAS*, 341, 33
 Kennicutt, R. C., Jr. 1998, *ARA&A*, 36, 189
 Koekemoer, A. M., Aussel, H., Calzetti, D., et al. 2007, *ApJS*, 172, 196
 Konno, A., Ouchi, M., Ono, Y., et al. 2014, *ApJ*, 797, 16
 Kunth, D., Mas-Hesse, J. M., Terlevich, E., et al. 1998, *A&A*, 334, 11
 Lai, K., Huang, J.-S., Fazio, G., et al. 2008, *ApJ*, 674, 70
 Mancini, C., Renzini, A., Daddi, E., et al. 2015, *MNRAS*, 450, 763
 McCracken, H. J., Milvang-Jensen, B., Dunlop, J., et al. 2012, *A&A*, 544, A156
 Mori, M., & Umemura, M. 2006, *Nature*, 440, 644
 Muzzin, A., Marchesini, D., Stefanon, M., et al. 2013, *ApJ*, 777, 18
 Nagao, T., Murayama, T., Maiolino, R., et al. 2007, *A&A*, 468, 877
 Nilsson, K. K., Möller, P., Möller, O., et al. 2007, *A&A*, 471, 71
 Ono, Y., Ouchi, M., Mobasher, B., et al. 2012, *ApJ*, 744, 83
 Ono, Y., Ouchi, M., Shimasaku, K., et al. 2010, *MNRAS*, 402, 1580
 Ouchi, M., Shimasaku, K., Akiyama, M., et al. 2008, *ApJS*, 176, 301
 Peng, C. Y., Ho, L. C., Impey, C. D., & Rix, H.-W. 2002, *AJ*, 124, 266
 Peng, Y.-j., Lilly, S. J., Kováč, K., et al. 2010, *ApJ*, 721, 193
 Renzini, A. 2009, *MNRAS*, 398, L58
 Sandberg, A., Guaita, L., Östlin, G., Hayes, M., & Kiaerød, F. 2015, arXiv:1501.06017
 Sanders, D. B., Salvato, M., Aussel, H., et al. 2007, *ApJS*, 172, 86
 Schaefer, D. 2003, *A&A*, 397, 527
 Schenker, M. A., Ellis, R. S., Konidaris, N. P., & Stark, D. P. 2014, *ApJ*, 795, 20
 Schinnerer, E., Smolčić, V., Carilli, C. L., et al. 2007, *ApJS*, 172, 46
 Schirmer, M., Diaz, R., Holmberg, K., Levenson, N. A., & Winge, C. 2013, *ApJ*, 763, 60
 Scoville, N., Aussel, H., Brusa, M., et al. 2007, *ApJS*, 172, 1
 Shibuya, T., Kashikawa, N., Ota, K., et al. 2012, *ApJ*, 752, 114
 Straatman, C. M. S., Labbe, I., Spitler, L. R., et al. 2015, arXiv:1506.01380
 Taniguchi, Y., Kajisawa, M., Kobayashi, M. A. R., et al. 2015, submitted to *PASJ*
 Taniguchi, Y., Scoville, N., Murayama, T., et al. 2007, *ApJS*, 172, 9
 van der Wel, A., Franx, M., van Dokkum, P. G., et al. 2014, *ApJ*, 788, 28